Title
MULTIFRAGMENTATION VERSUS SEQUENTIAL FISSION: OBSERVABLE DIFFERENCES?

Authors
Lopez, J.A.
Randrup, J.

Publication Date
1988-08-01

LBL-25664
Preprint

Lawrence Berkeley Laboratory
UNIVERSITY OF CALIFORNIA

Submitted to Nuclear Physics A

Multifragmentation versus Sequential Fission: Observable Differences?

J.A. López and J. Randrup

August 1988

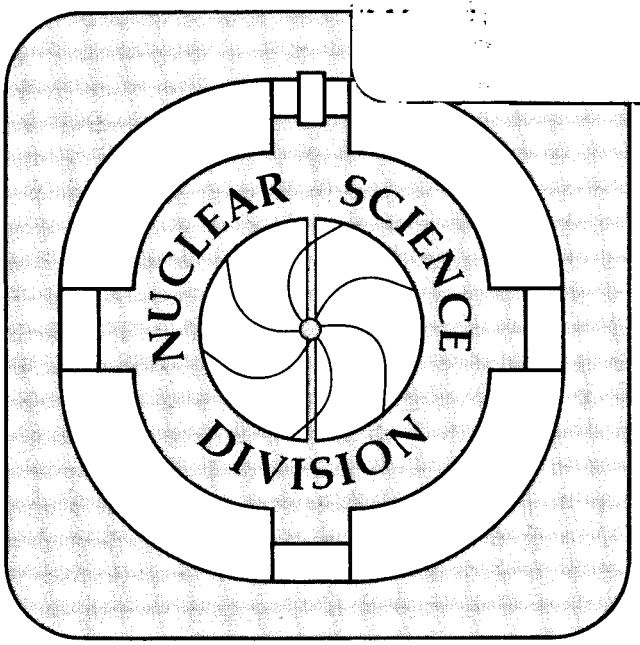

Prepared for the U.S. Department of Energy under Contract Number DE-AC03-76SF00098.

DISCLAIMER

LBL-25664

Multifragmentation versus Sequential Fission: Observable Differences?

Jorge A. López and Jørgen Randrup

Nuclear Science Division, Lawrence Berkeley Laboratory
University of California, Berkeley, California 94720

August 7, 1988

Abstract:

To elucidate the observable distinctions between different reaction mechanisms for multifragment production in nuclear collisions at intermediate energies, we contrast two opposite extremes: sequential binary fission and simultaneous multifragment breakup (*true* multifragmentation). For identical multifragment channels produced by these two idealized mechanisms, we examine the kinetic-energy spectra and the correlated velocity distributions of the fragments and discuss the possibility of identifying informative multifragment observables.

*This work was supported in part by the Director, Office of Energy Research, Division of Nuclear Physics of the Office of High Energy and Nuclear Physics of the U.S. Department of Energy under Contract No. DE-AC03-76SF00098.

1 Introduction

Nuclear collisions at intermediate energies present unique possibilities for probing the properties of hot and dense nuclear matter. However, the extraction of unambiguous information depends on our ability to discern the reaction mechanisms in play. This is no easy task, since these collisions typically lead to final states containing many complex and excited fragments. Moreover, the dependence of the reaction dynamics on the (uncontrollable) impact parameter acts to further obscure the basic phenomena. This inherent complexity makes it difficult to interpret experimental data on multifragmentation processes. The difficulty is compounded by the fact that a plethora of models exist for nuclear collisions at intermediate energies, and typically the (limited) data available can be accounted for by models based on mutually conflicting assumptions.

With the aim of identifying observables that may help to elucidate the underlying reaction dynamics, we have examined the kinematical differences between two opposite extremes, namely sequential binary fission and *true* multifragmentation, *i.e.* simultaneous multifragment breakup. We first give a brief description of these models and the generation of ensembles of multifragment events. Subsequently, we consider a number of observables and discuss their utility as discriminators between different disassembly mechanisms. We conclude with some suggestions for the design and analysis of multifragmentation experiments.

2 Models

We consider the disassembly of an idealized nuclear "source", as may be formed in a nuclear collision at intermediate energy. In its CM frame, such a source is characterized by its baryon number A, charge number Z, and energy E, as measured relative to the rest energy of its A individual constituent nucleons.

2.1 Sequential Binary Decay

In the first extreme, the source is considered as a compound nucleus and is assumed to disassemble by sequential binary decay. We shall refer to any such split as a "fission" process, although *all* possible binary channels are considered, ranging from symmetric fission to nucleon evaporation. In general, the binary split produces two new compound nuclei which may then undergo further binary decay, provided that their excitation energy is high enough. This tree of fission processes results in a final multifragment state consisting of individual nucleons and bound complex nuclear fragments.

For the total level density of a compound nucleus with mass number A, charge number Z, and energy E we employ the simple form

$$\rho(A,Z,E) = \frac{k}{\sqrt{A}}\, \mathrm{e}^{2\sqrt{a_A E^*}} \,, \tag{1}$$

where $E^\star$ is the intrinsic excitation energy of the nucleus, equal to E plus the binding energy of the ground state. The preexponential mass dependence is chosen so that the correct limiting behavior for very large systems is obtained.[1] A reasonable reproduction of the global trends throughout the nuclear chart is obtained with the value $k = 0.002$ MeV^{-1}. The level density parameter a_A is taken from the study by Tōke and Świątecki [2],

$$a_A = \frac{A}{14.61 \text{ MeV}} \left(1 + 3.114\ A^{-\frac{1}{3}} + 5.626\ A^{-\frac{2}{3}}\right) . \tag{2}$$

Now consider a specific binary decay, $A_0Z_0E_0 \rightarrow A_1Z_1E_1 + A_2Z_2E_2$. According to the canonical transition state method, the corresponding decay width is given by

$$d\Gamma_{12} = \frac{\rho_{12}(A_0, Z_0, E_0 - K_0^{12} - B_0^{12})}{\rho_0(A_0, Z_0, E_0)}\ dK\ , \tag{3}$$

where K is the asymptotic kinetic energy of the relative fragment motion. The level density of the activated nucleus at the conditional saddle point for the particular mass-asymmetry considered is denoted by $\rho_{12}(E_0^{12})$. Here the intrinsic excitation energy of the nucleus at the saddle point is given by $E_0^{12} = E_0 - K_0^{12} - B_0^{12}$, where B_0^{12} is the barrier height and K_0^{12} denotes the kinetic energy of relative motion of the two (pre)fragments at the saddle point. The conditional barrier B_0^{12} is calculated by a recently improved version of Swiatecki's [3] global description of particle emission (see ref. [1] for details). Furthermore, in the present study, a given decay is only allowed if K_0^{12} is positive, *i.e.* if the particular fission channel must be classically allowed. Inclusion of the quantal transmission coefficient and integration over K yields the usual Bohr-Wheeler result for fission, averaged over the fragment excitation energies.

To estimate the level density of the activated complex, we assume that the saddle configuration is of dinuclear form, as is approximately the case for the lighter nuclei typically involved. We then have

$$\begin{aligned} \rho_{12}(A_0, Z_0, E_0^{12}) &\approx \int dE_1' \int dE_2'\ \delta(E_1' + E_2' - E_0^{12})\ \rho_1(A_1, Z_1, E_1')\ \rho_2(A_2, Z_2, E_2') \\ &\approx \frac{\sqrt{a_1 a_2}}{a_1 + a_2}\ \sqrt{4\pi\tau_{12}E_0^{12}}\ \rho_1(A_1, Z_1, E_1)\ \rho_2(A_2, Z_2, E_2)\ . \end{aligned} \tag{4}$$

The last result is obtained by applying the stationary-phase approximation to the energy convolution. The mean excitation energies in the daughter fragments are then given by $E_i = E_0 a_i/(a_1 + a_2)$, $i = 1, 2$, where a_i are the corresponding level-density parameters (see eq. (2)), and the intrinsic temperature of the transition configuration is determined by $E_0^{12} = (a_1 + a_2)\tau_{12}^2$.

The above approximations yield the following simple expression for the decay widths,

$$d\Gamma_{12} \approx k\ \frac{\sqrt{a_1 a_2}}{a_1 + a_2}\ \sqrt{4\pi\tau_{12}E_0^{12}}\ \sqrt{\frac{A_0}{A_1 A_2}}\ \mathrm{e}^{2\sqrt{a_1 E_1} + 2\sqrt{a_2 E_2} - 2\sqrt{a_0 E_0}}\ dK\ . \tag{5}$$

On the basis of this expression, a random selection is made of the actual decay channel. The magnitude of the asymptotic fragment momenta follows by energy conservation and the direction of motion is picked randomly of 4π, in the CM frame of the decaying system. The decay procedure is then iterated for each daughter fragment, until stability is reached. In this manner, an ensemble of final multifragment events is conveniently generated.

2.2 Multifragmentation

The above mechanism of sequential binary decay is rather well defined. We wish to contrasts it with the mechanism of simultaneous multifragment breakup, which may be referred to as *true* multifragmentation. In order to facilitate the comparison, we wish to compare events that differ only kinematically, *i.e.* contain the same fragment species. For this purpose, we devise a scheme that produces a multifragmentation event for each event generated by the sequential-binary mechanism described above. The partner event consists of the exact same fragments, and has the same total energy, but the individual fragment velocities are different. In this manner the inherent kinematical differences between the two mechanisms can be brought out most clearly.

For a given sequential-fission event, its multifragmentation partner event is generated by repositioning all the final sequential-fission fragments randomly within a small spherical (freeze-out) volume and then following their trajectories as they disassemble under the influence of their mutual Coulomb repulsion. Any reasonable multifragmentation model will produce unstable primary fragments that subsequently undergo evaporation on a slower time scale. This is taken into account in a rough manner by temporarily stopping the fission process whenever the decaying compound system has an excitation below 50 MeV and then performing the simultaneous breakup with these excited fragments. Subsequently, after the fragments have separated they are allowed to continue their deexcitation by the same processes as applies to the sequential-fission products.

The initial multifragmentation process is prepared as follows. The excited fragments are placed in a random non-overlapping configuration with their centers confined within a sphere whose volume is twice that of the nuclear volume for the original compound nucleus A_0Z_0. (The specific value of two is somewhat arbitrary, but this is of little importance in the present study.) For the resulting configuration, the potential energy V associated with the mutual Coulomb repulsion between the fragments is then calculated. (If it exceeds the total kinetic energy in the event, K_∞, the configuration is expanded uniformly until $V = K_\infty$.) After the fragments have been thus positioned, the excess energy, $K = K_\infty - V$, is distributed among the translational degrees of freedom of the fragments. This is accomplished by first picking preliminary fragment momenta from a Maxwell distribution with temperature $\tau = K/[\frac{3}{2}(N-1)-1]$, then performing an overall Galilei boost so as to ensure that the total momentum of the N fragments vanish, and finally renormalizing the

fragment momenta by a common factor so as to match the available kinetic energy K. This "freezeout" state is then propagated dynamically, under the action of the Coulomb repulsion, until the fragments have attained their asymptotic velocities. Finally, the excited particles are allowed to de-excite by evaporation producing a mass distribution identical to that of the corresponding sequential-decay event.

The event samples produced in this simple statistical multifragmentation model match, event by event, those produced by the sequential mechanism, with respect to total kinetic energy, fragment composition, and fragment excitation. The cost of the simplicity of this model is the separation of the Coulomb expansion and the final evaporation of the fragments. However, based on the calculations in ref. [4], we do not expect that this approximation will affect the results drastically.

3 Illustrative Results

To set a framework for our comparison we concentrate on the system $A = 150$, $Z = 62$ mainly at excitation energy $\epsilon = 5$ MeV/N, although the cases at 2 and 10 MeV/N have also been calculated. A similar case has been studied both experimentally and theoretically [5]. Figure 1 shows the mass yields obtained for these three cases. These multiplicities point to light particle evaporation as the main decay channel at low energies, and to more symmetrical fission decay at higher energies; this will be studied quantitatively in ref. [1]. For $\epsilon = 5$ MeV/N the mean number of fragments was found to be ≈ 55 (including nucleons) and the three heaviest fragments have masses of 52.3 ± 9.1, 32.1 ± 7.9 and 10.2 ± 3.2, respectively.

3.1 Proton Energy Spectra

As a first comparison between sequential binary fission and multifragmentation we consider the distribution of the proton energy. Figure 2 shows the spectra corresponding to these two breakup mechanisms. In both cases a Coulomb peak is clearly visible. For fission, since the protons are emitted from fission partners and other smaller fragments varying in mass, the peak is broader and corresponds to a smaller total charge than in multifragmentation where the protons feel all the charges simultaneously.

The two-component shape of the curves, on the other hand, reflects the existence of two sources of evaporated protons. At low energies the protons come from slowly moving heavy sources, while at higher energies they originate from rapidly moving light particles. The long tail observed at high energies is reminiscent of that obtained in proton-induced fragmentation [6].

3.2 Velocity Distribution

Additional information on the origin of the different Coulomb peaks can be obtained by relating the proton velocities to the velocities of heavier fragments, *i.e.* to their

sources. We do this by plotting the velocities of the final fragments in the three-dimensional velocity space. To allow a superposition of results from different events we first normalize the velocities by dividing by the mean fragment speed $\bar{v}$ for the particular event. We then plot them in a coordinate system in which the largest fragment is at the origin, the second largest is on the positive v_x axis, and the third largest is in the upper half v_x-v_y plane. Figure 3 shows the superposition of 250 events for $\epsilon = 5$ MeV/N. (Be aware that that this figure includes the neutrons which are most often not observed.)

In fig. 3*a*, corresponding to sequential binary decay, the sources of the evaporated light particles are seen to be the largest (at the origin) and second largest (along the positive v_x-axis) fragments, presumably fission partners. The spreading of the clouds around the second largest fragment is due to different fission asymmetries. The rest of the particles can be related to subsequent decays. In striking contrast, the multifragmentation result (fig. 3*b*) is dominated by a single distribution around the CM velocity of the entire system (located between the heaviest and second largest fragments).

The proton spectra for the sequential binary decay can now be understood as coming from evaporation from the two heaviest sources, whereas the multifragmentation curve mainly reflects a single distribution observed around the CM velocity.

3.3 Velocity Correlations

One can obtain a quantitative estimate of these different velocity distributions by calculating a particle correlation function in velocity space. This can be done in several ways. Here we discuss a method adapted from condensed-matter physics and define the velocity correlation function $g(v)$ by

$$g(v)\ n_0\ 4\pi v^2 dv = dn(v)\ . \tag{6}$$

Here $dn(v)$ is the number of fragment pairs with a relative speed equal to the specified amount v, to within a tolerance of dv. Furthermore, n_0 is the characteristic density of fragments in velocity space; this normalization constant is taken as the number of fragments with a speed less than $\frac{6}{5}\bar{v}$, divided by $\frac{4}{3}\pi\bar{v}^3$, where $\bar{v}$ is the mean speed of the fragments. [In condensed-matter problems, v is replaced by the radial separation and n_0 is the mean spatial density. Since the fragment gas is not uniform in velocity space, the definition of n_0 is ambiguous. Fortunately, this causes no essential problem, since n_0 only serves to achive a convenient overall normalization.] Thus, the function $g(v)$ measures the radial distribution of neighbors in velocity space, relative to an uncorrelated uniform distribution.

We now employ the above method to bring out the velocity correlation existing among the produced fragments. Fig. 4*a* displays the correlation function $g(v)$ when *all* the produced fragments are included. The resulting velocity correlation shows an striking difference between the two disassembly mechanisms under consideration. Again, the result obtained for the sequential binary decay reflects the light-fragment

clouds around the heavy fragments as a proniounced cloud-to-cloud correlation at $v \approx \bar{v} \approx 0.075c$. The multifragmentation curve, on the other hand, shows only a smooth increase in correlation for small velocity differences, as expected for the single velocity distribution of fig. 3*b*.

Figure 4*b* shows the corresponding results when only charged fragments are included in the analysis, and fig. 4*c* is the result when only heavy fragments ($A > 4$) are considered. For both disassembly mechanisms, these two sets of results continue to exhibit an enhanced velocity correlation for two heavy fragments, but fail to show pronounced differences between the two mechanisms.[1]

One could try to further quantify these differences by comparing the sum of the inverse of the velocity differences in the two models, *i.e.* by calculating $H = \sum \bar{v}/v$ with the sum running over all fragment pairs. Since the inverse velocity assigns more weight to smaller velocities, the sequential breakup is expected to yield a larger value for this function than multifragmentation; indeed, we find $H_{\rm sf}/H_{\rm mf} \approx 4.75$ for $\epsilon = 5$ MeV/N.

3.4 Shapes of Velocity Distributions

Another noticeable difference of the velocity distributions is the distinct shape of the envelopes of the two cases. The two clouds present in fig. 3*a* have a more elongated shape for the sequential decay than the relatively spherical shape for the simultaneous breakup. To study these structures we perform an sphericity analysis [8] for each of these events.

Thus, we consider the kinetic-flow tensor

$$F_{ij} = \sum_n \frac{p_i^{(n)} p_j^{(n)}}{2m_n} , \qquad (7)$$

where $p_i^{(n)}$ denotes the $i^{\rm th}$ Cartesian component of the momentum of the $n^{\rm th}$ fragment and m_n is its mass. One can use the ordered eigenvectors of F, $t_1 < t_2 < t_3$, to define the reduced quantities $q_i \equiv t_i^2 / \sum_{j=1}^3 t_j^2$, in terms of which the sphericity and coplanarity shape parameters are given by $S = \frac{3}{2}(1 - q_3)$ and $C = \frac{1}{2}\sqrt{3}(q_2 - q_1)$, respectively. In this $S - C$ plane the origin would correspond to a rod-like object, the point $(1, 0)$ to a spherical shape, and $(\frac{3}{4}, \frac{\sqrt{3}}{4})$ to a disk.

Figure 5 presents the result of this analysis for 200 events. The differences in shape are clearly visible, with the sequential binary decays having a rod-like shape and the multifragmentation results being more spherical.

[1] It is particularly noteworthy that the correlation among the heavy fragments (fig. 4*c*) yields very similar results for the two different breakup mechanisms. This type of correlation has recently been investigated experimentally and the results have been interpreted as evidence of simultaneous multifragmentation [7]. However, in view of our present results, it appears that the velocity correlation does not uniquely distinguish between the sequential and simultaneous modes of multifragment production.

3.5 Folding Angle

A direct consequence of these different shapes of the velocity distributions is the angular correlation of the two heaviest fragments of each event. This angle is a natural generalization of the folding angle commonly employed in ordinary fission studies. For the sequential binary breakup we expect that the two largest fragments mostly arise as residues of two early fission partners and therefore tend to appear back to back, whereas these heavy fragments are expected to have a broader angular distribution for the simultaneous breakup mechanism.

In fig. 6 we present the distribution of the angles between the two heaviest fragments of each of 500 events as obtained for the two breakup mechanisms considered. As expected for a fission process, the two largest fragments in the sequential mechanism are highly correlated at large angles and appear to have been emitted almost back to back. The simultaneous process, on the contrary, peaks around 140° with a wider distribution. This brings out the different geometry characterizing the two mechanisms of fragment production.

4 Discussion

In the preceding section we have highlighted the kinematical differences between the two opposite breakup mechanisms considered. In addition to the differences in Coulomb peaks for the proton distribution, we found that the mechanisms differ markedly in velocity correlations, sphericity-coplanarity coordinates, and heavy-fragment angular correlations. Unfortunately, we also find these differences to be energy dependent and difficult to pinpoint experimentally, in addition to being somewhat model dependent. In the present section we discuss these problems and attempt to relate our findings to current research efforts in this direction.

4.1 Excitation Energy Dependence

So far we have concentrated our discussion on intermediate source excitations, namely $\epsilon = 5$ MeV/N. At both higher and lower energies the differences found in the previous section change qualitatively and quantitatively, as one would expect.

As shown in fig. 1, at low energies (*e.g.* 2 MeV/N) the main mode of de-excitation appears to be light-particle evaporation. An immediate consequence of this is the absence of a second heavy fragment source of evaporated particles. This, in effect, generates a single velocity cloud much like the multifragmentation one washing away the strong kinematical signatures seen in the previous section.

This merging of the two mechanisms at low energies is to be expected. Accepting the fact that the timing of fragment production is the main difference in our two models, it is easy to see that the models will coincide when the multiplicity of heavy fragments decreases to two or one. Furthermore, the Coulomb effects at this low multiplicities will be exactly the same in the two cases giving a back-to-back push

between heavy fragments and since both mechanisms split a compound nucleus, source velocity studies as those of Bowman *et al.*[5] and Moretto and Wozniak [9] are bound to describe the binary nature of the fragment production.

At higher energies (*e.g.* 10 MeV/N) the signatures again weaken, but for different reasons. In the sequential-decay model, the occurrence of more than two heavy fragments coming from succesive symmetric fissions introduces additional sources of evaporated light particles, which smear the velocity distribution so that it appears more similar to that of the multifragmentation mechanism. In this connection, it should be noted that for higher excitation energies, the heavy-fragment multiplicity of the sequential binary decay model increases (*cf.* fig. 1), as it would for multifragmentation. Consequently, this effect can *not* be interpreted as a signature for simultaneous breakup as has been suggested in the literature [10].

4.2 Caveats

It is important to note that although our calculations indicate that the velocity correlations between all particles (*cf.* fig. 4*a*) could be used as a guide to distinguish between the opposite mechanisms, the experimental observation of these correlations is difficult as it involves observation of (nearly) all the fragments (including neutrons) for each event. As seen in the parts *b* and *c* of fig. 4, restriction to charged or heavy fragments only reduces the differences between the correlation functions and makes the identification of the disassembly mechanism more difficult.

Moreover, it has been a tacit assumption of our comparison that multifragmentation produces the same mass distribution as sequential-binary decay for a given excitation energy. Our results will be directly relevant if the experimental yields resemble the ones calculated here. If the measured multifragment yields turn out to be very different from those calculated, this difference by itself might be used to identify the breakup mechanisms.

4.3 Concluding Remarks

In the present work, we have studied the possibility of discriminating between different multifragmentation mechanisms by means of kinematical observables, *i.e.* quantities derived from the velocities of the observed fragments. For this purpose, we considered two opposite extremes: sequential binary decay and simultaneous multifragment breakup. For these idealized mechanisms, several noticeable differences arise and their origins have been discussed.

The consideration of the folding-angle distribution appears particularly promising, since it is rather simple (both conceptually and practically) and relates directly to the heavy fragments. Furthermore, the velocity-distribution plot may be a useful discriminator between the different disassembly mechanisms, provided that (nearly) all fragments (including the neutrons) are observed. Despite the considerable practical problems associated with multifragment and neutral-particle detection, such experiments are now becoming feasible and we hope that the present study may

provide some inspiration, both in the design of the experiments and for the data analysis.

In the present study we have deliberately limited our considerations to *kinematical* correlations, by comparing classes of events that are matched, pair by pair, with respect to both fragment species and total four-momentum. In a more complete study, it must be investigated how the fragment species distribution is affected by the specific disassembly mechanism. Such an endevour involves generalizing the relatively unique formalism for binary decay to breakup of higher multiplicity (ternary, quaterny, ...). We are currently pursuing this problem and will report on our progress in due course [1].

This work was supported in part by the Director, Office of Energy Research, Division of Nuclear Physics of the Office of High Energy and Nuclear Physics of the U.S. Department of Energy under Contract No. DE-AC03-76SF00098.

References

[1] J.A. López and J. Randrup, in preparation.

[2] J. Tōke and W.J. Świątecki, Nucl. Phys A372 (1981) 141.

[3] W.J. Świątecki, LBL report 11403 (1983), unpublished.

[4] H.W. Barz, J.P. Bondorf, and H. Schulz, Nucl. Phys A462 (1987) 742; K.C. Chung, R. Donángelo, and H. Schechter, Phys. Rev. C36 (1987) 986.

[5] D.R. Bowman *et al.*, Phys. Lett. B 189 (1987) 282; D.H.E. Gross, Phys. Lett. B 203 (1988) 26.

[6] A.S. Hirsch *et al.*, Phys. Rev. C29 (1984) 508.

[7] J. Pochodzalla *et al.*, Proceedings of the Third International Conference on Nucleus Nucleus Collisions, Saint-Malo, France, (1988) 96; G. Klotz-Engmann *et al.*, ibid, 60.

[8] M. Gyulassy, K.A. Frankel, and H. Stöcker, LBL-13379 (1981), unpublished.

[9] J. Gomez Del Campo, Phys. Rev. C19 (1979) 2170; F. Auger *et al.*, Phys. Rev. C35 (1987) 190; L.G. Moretto and G.J. Wozniak, LBL-24558 (1987), submitted to Progress in Particle and Nuclear Physics.

[10] R. Trockel *et al.*, Contributed Papers, Third International Conference on Nucleus Nucleus Collisions, Saint-Malo, France, (1988) 86; R. Bougault *et al.*, *ibid*, 83; G.M. Jin *et al.*, *ibid*, 77.

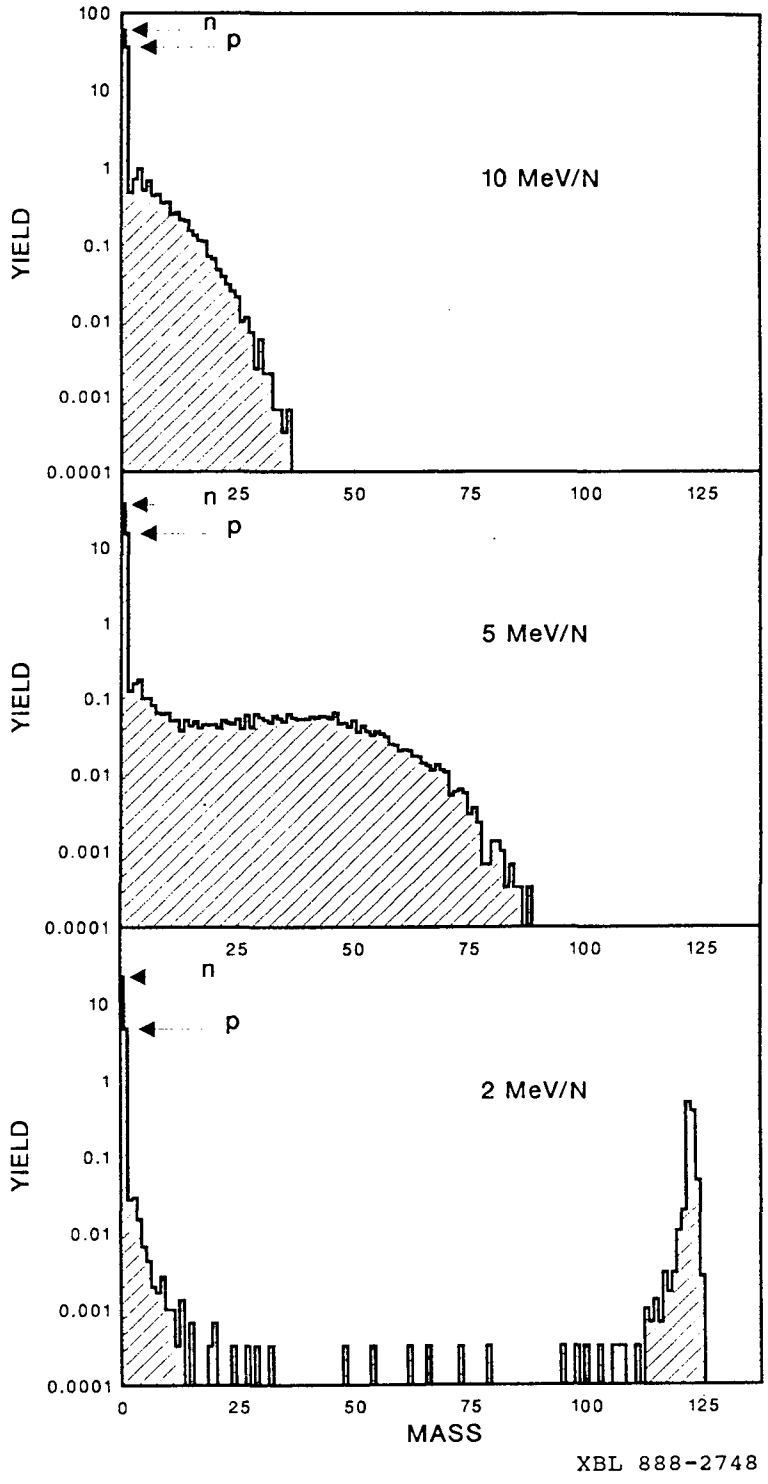

Figure 1: Mass Yield

Relative yields of fragments with a given mass number A, as obtained from 3000 events of the sequential binary decay model for the system $A = 150$, $Z = 62$ and for excitation energies of 2, 5 and 10 MeV/N. Neutrons are included to the far left of the plot in the first column as denoted by the arrow.

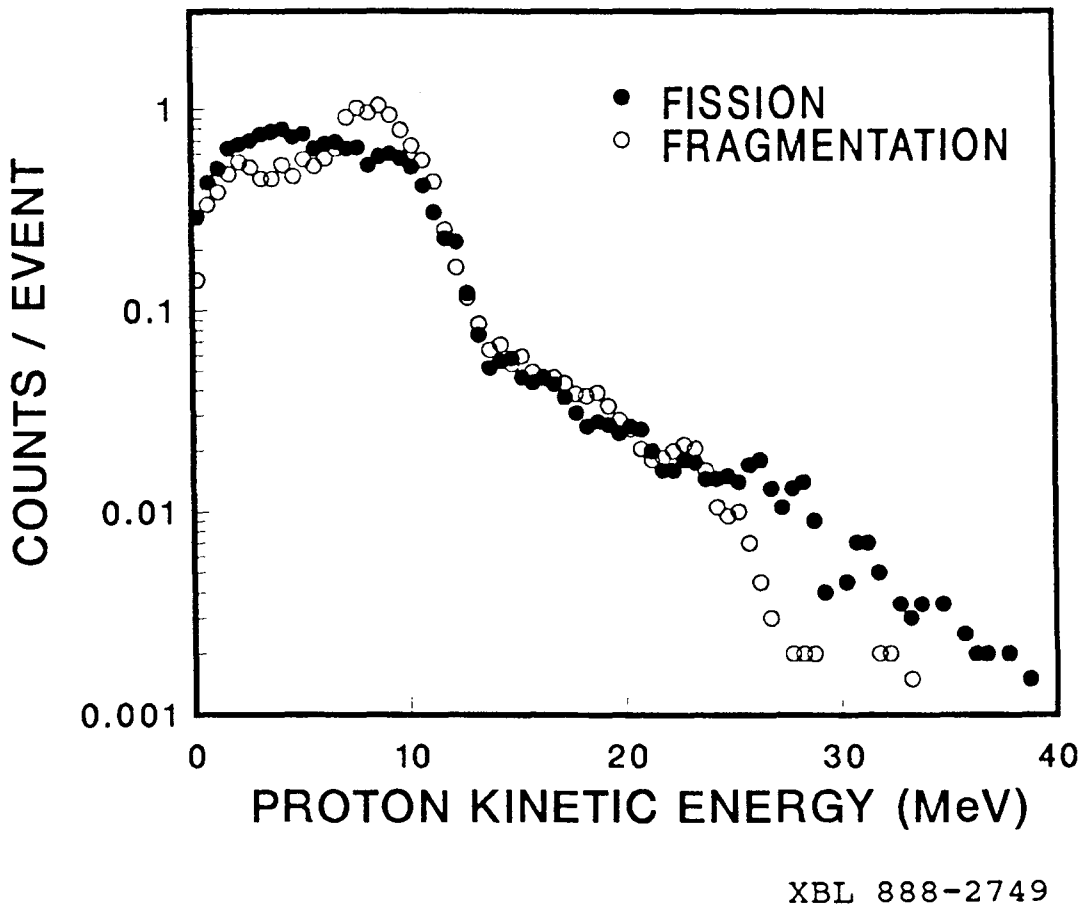

Figure 2: Proton Energy Spectra

Proton energy spectra obtained in 500 events of the sequential binary decay (solid circles) and multifragmentation (open circles) models for $A = 150$, $Z = 62$ and $\epsilon = 5$ MeV/N.

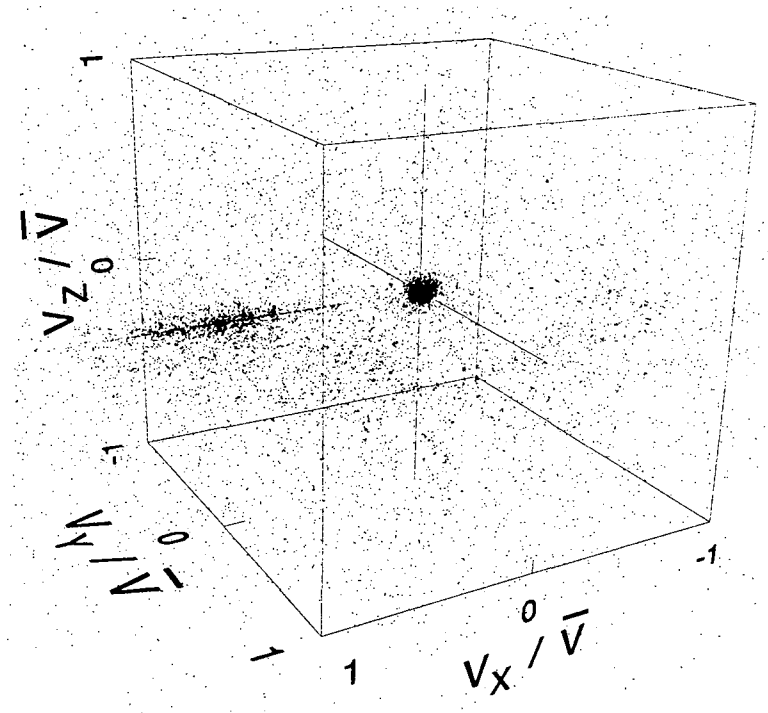

XBL 888-2750

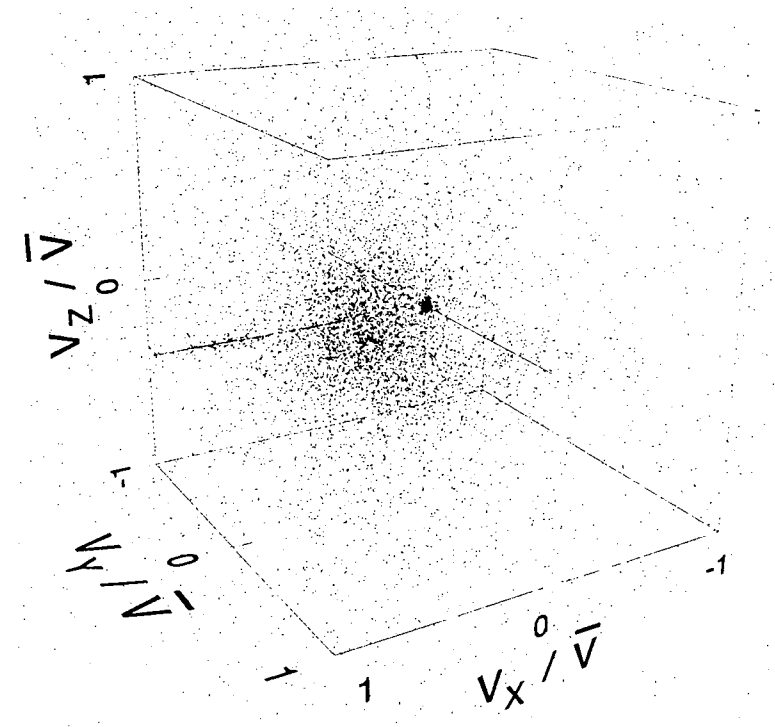

XBL 888-2751

Figure 3: Velocity Distributions

Superposition of all the fragment velocities for 250 events generated by either sequential binary decay (a) or multifragmentation (b), for $A = 150$, $Z = 62$, $\epsilon = 5$ MeV/N. In this representation, the three largest fragments are located at the origin, along the positive v_x axis, and in the upper half $v_x - v_y$ plane, respectively.

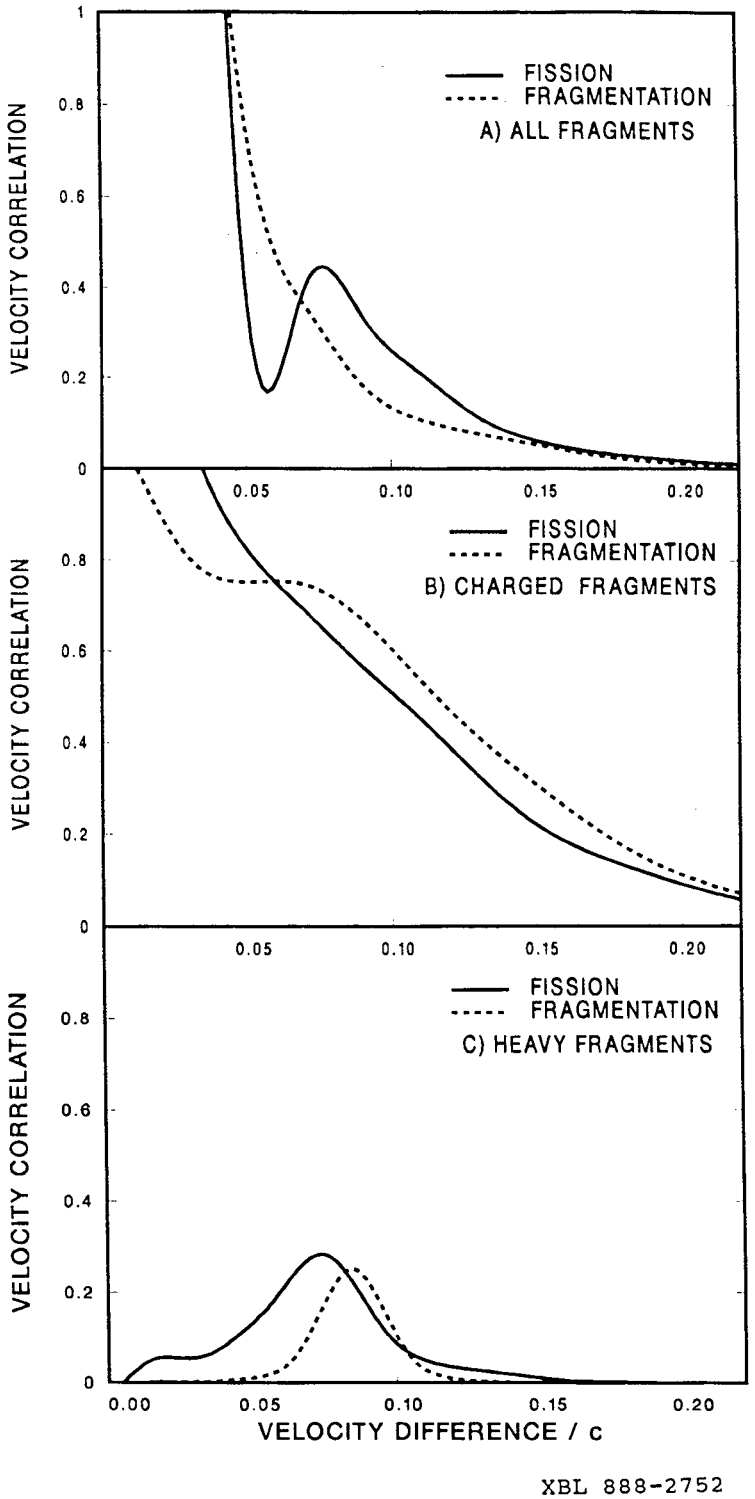

Figure 4: Velocity Correlations

Fragment-velocity correlation functions for a) all fragments b) charged fragments only and c) heavy fragments ($A > 4$) only. $A = 150$, $Z = 62$, and $\epsilon = 5$ MeV/N. The increased correlation observed in the result for all fragments for the sequential binary decay at $v \approx \bar{v} \approx 0.075c$ reflects the presence of the clouds observed in the previous figure.

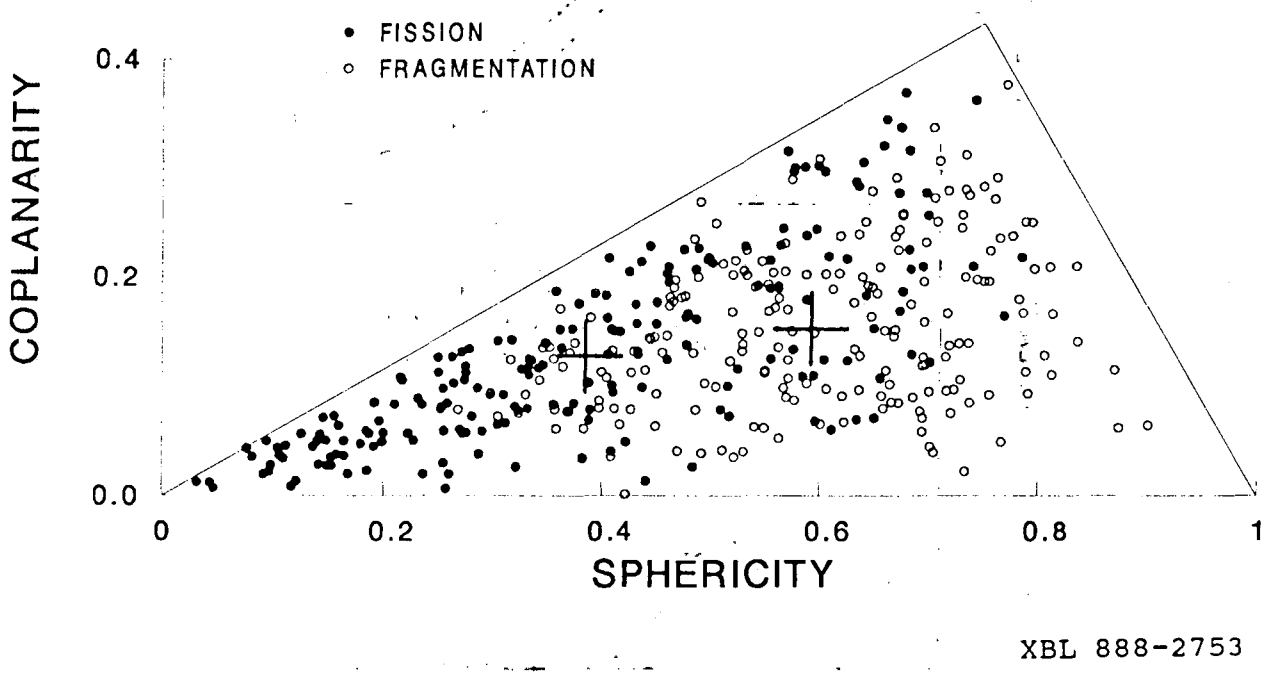

Figure 5: Event Shape

Superposition of 200 events in the sphericity-coplanarity plane for $A = 150$, $Z = 62$, and $\epsilon = 5$ MeV/N. The sequential binary decay events appear to be elongated and the multifragmentation ones more spherical. This is also reflected by the average sphericity and coplanarity of the sequential decay (left cross) and simultaneous breakup (right cross).

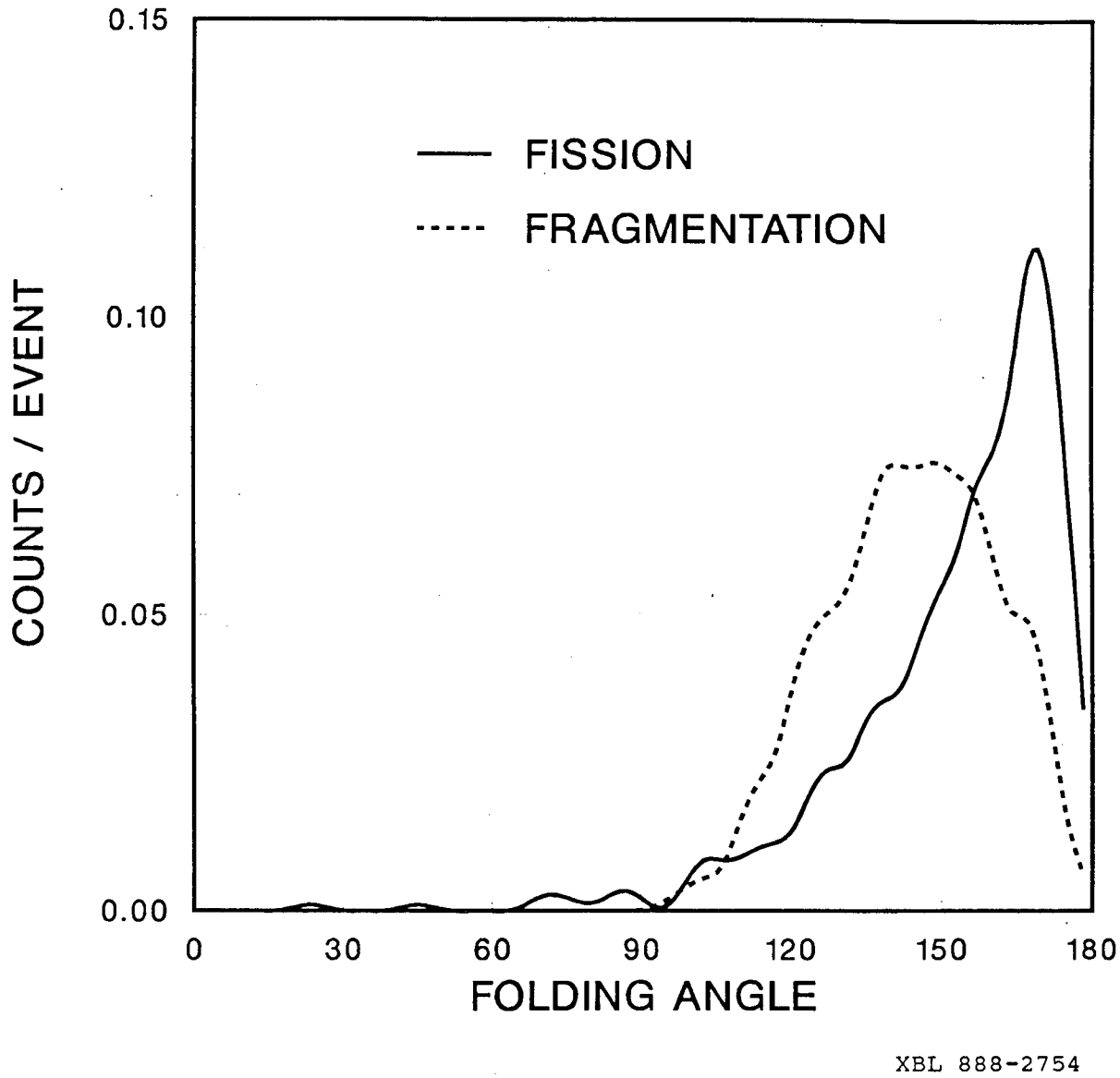

Figure 6: Folding Angle

Distribution of the asymptotic angles formed by the two heaviest fragments in each of 500 events. Sequential decay products appear to have been emitted nearly back-to-back, whereas the simultaneous breakup leads to folding angles peaked around 140°.

LAWRENCE BERKELEY LABORATORY
TECHNICAL INFORMATION DEPARTMENT
UNIVERSITY OF CALIFORNIA
BERKELEY, CALIFORNIA 94720